An Application of Adaptive Blades on Convertible MAVs

Peng Lv, Fazila Mohd Zawawi, Emmanuel Bénard, Sebastien Prothin,
Jean-Marc Moschetta, Joseph Morlier

An Application of Adaptive Blades on Convertible MAVs

Peng Lv, Fazila Mohd-Zawawi, Emmanuel Benard, Sebastien Prothin, Jean-Marc Moschetta and Joseph Morlier
Institut Supérieur de l'Aéronautique et de l'Espace, University of Toulouse, France

ABSTRACT
A passive twist control is considered as an adaptive way to maximize the overall efficiency of a proprotor developed for convertible Micro Air Vehicles. The varied operation conditions suggest different twist distributions for hover and forward flight with the constraint of identical planform. In this work, adaption of the proprotor geometry is achieved by centrifugal force induced twist. Classical Lamination Theory is used to predict structural loads, while Blade Element Momentum Theory is employed to understand the aerodynamic benefits of adaptive proprotor as applied on Micro Air Vehicles. Tip mass is proposed to increase the stability and generate negative torsion for rotating blade. Validation of the procedure is based on measurements of blade deformation, performed by laser displacement sensors. While negative torsion is found in both rotor and propeller modes, level of deformation is still below what is required for optimum dual operation.

1. INTRODUCTION
Convertible rotor aircraft has been developed for versatility services for several years, as it combines the merits of a helicopter and airplane. It has the capacity of Vertical/Short TakeOff and Landing (VSTOL) like a helicopter, through tilting rotor, then converts to forward flight at relatively high speed, as an airplane. The three main convertible rotor configurations are the tilt-rotor, tilt-wing and tilt-body. Tilt-rotor aircraft was developed in early 1950s, exemplified by the Bell XV-3 operating the first transition from hover to forward flight. In 1970s, XV-15 demonstrated the feasibility of tilt-rotor concept. The success of XV-15 led to the V-22 project, leading to the first production tilt-rotor aircraft in the world. Recently, the tilt concept has attracted the attention of MAV research community. In 2008, Shkarayev and Moschetta introduced the concept of tilt-body MAV, which has a tilt-body configuration and is capable of flying in hover and forward flight [1]. This configuration of tilt-body MAV was successfully tested in flight.

Designing a proprotor to operate efficiently in hover and forward flight presents a challenge since the inflow velocity and thrust requirement for each flight condition are quite distinct. In hover, the inflow velocity is small and the proprotor must provide high thrust to support the aircraft weight. By contrast, in forward flight, the inflow velocity is relatively large and the low thrust must only overcome the drag. The difference in the inflow and thrust requirements between the two flight modes suggests different blade twist and chord distributions. In terms of twist effect on efficiency, high blade twist on the proprotor allows the aircraft to fly faster and more efficiently, whereas low blade twist increases the efficiency in hover. In 1983, McVeigh obtained the twist of XV-15 proprotor through linear interpolation of twist between ideal rotor and propeller by a compromise analysis [2]. Although this trade-off solution provided an acceptable performance on XV-15, the stiff proprotor with certain twist cannot maximize the efficiency for both flights. In 1988, Nixon proposed a passive blade twist control for the proprotor on XV-15 [3]. The study demonstrated successfully the feasibility of the passive blade control on conventional tilt-rotor aircraft. The small proprotors also suffer the problem caused by different twist between hover and forward flight. However, due to the small size of MAV, the complex tailored cross section of blade for passive twist control based on conventional tiltrotor aircraft is not available any more.

In this paper, a numerical method is employed to obtain the optimal twist distributions of proprotor. In order to achieve the varied twist, the concept of centrifugal force induced twist will be introduced as

a more practical method for proprotor of MAV. Then, the deformation of rotating laminate blade is measured using laser displacement sensors. Finally, this concept is assumed to be applied on a MAV and the potential benefits are evaluated using Blade Element Momentum Theory model.

2. OPTIMAL BALDE TWIST OF MAVION

2.1 Mission of MAVion

MAVion, a tilt-body MAV developed by ISAE, is designed to fly in both hover and forward flight, as shown in Fig. 1. The typical wing Reynolds number of its operation conditions is below 100,000. In hover mode, the nominal thrust 2N to support the weight while it becomes 0.3N to balance the drag in forward flight.

Figure 1: The MAVion, a convertible MAV developed in ISAE

Table 1: MAVion properties

Wingspan (m)	Airfoil	Wing Area (m^2)	Aspect Ratio	Aileron Area (m^2)
0.36	MH45	0.0792	1.64	0.0216

Table 2: Mission of MAVion

	Hover	Forward flight
Inflow velocity (m/s)	0	16
RPM	11,000	11,000
Thrust (N)	2	0.3

2.2 Optimum twist distributions in hover and forward flight

For a blade rotating in a free-stream with the rotational plane perpendicular to the flow direction, the optimum performance is realized when the blade twist distribution is such that the Betz condition is satisfied [3, 8]. The Betz condition describes that the trailing vortex sheet moves aft as a rigid helical sheet, which means the wake displacement velocity is radically constant. Using Blade Element Momentum Theory (BEMT) to satisfy the Betz condition, the displacement velocity of the vortex sheet

can be approximately expressed by:

$$\upsilon_0 = \frac{\omega R}{2}(\sqrt{\mu^2 + 2C_T} - \mu) \tag{1}$$

Where ω is rotational velocity, R is the blade radius, μ is tip speed ratio which is defined by inflow velocity V, rotational velocity ω and blade radius R, $\mu = \frac{V}{\omega R}$, C_T is the thrust coefficient. Furthermore, the optimum blade twist distribution is:

$$\theta = \tan^{-1}\left(\frac{\upsilon_0}{\omega r} + \mu\frac{R}{r}\right) + \alpha_{opt} \tag{2}$$

Where r is the local radius, α_{opt} is the optimum angle of attack in terms of lift-drag ratio.For a radically constant chord and airfoil section, α_{opt} can be ignored since it is always the same for each of blade element. It cannot influence the built-in twist of blade. According to Tab. 2, the optimum twist distributions of MAVion were calculated using Eqs. 1 and 2, which are shown in Fig. 2.

In order to distinguish the twist distributions, they were plotted by the translations in Y axis direction so that the twist in each mode at 0.75R is 0. With respect to the built-in twist, it shows nonlinear with around –35˚ twist from blade root to tip. By contrast, the twist distribution in hover is shown to be highly nonlinear with –15˚ twist from blade root to tip. Hence, different flight modes suggest varied built-in twist distributions of blade. The solution is to find an adaptive proprotor which can deform in twist and adapt different flight conditions.

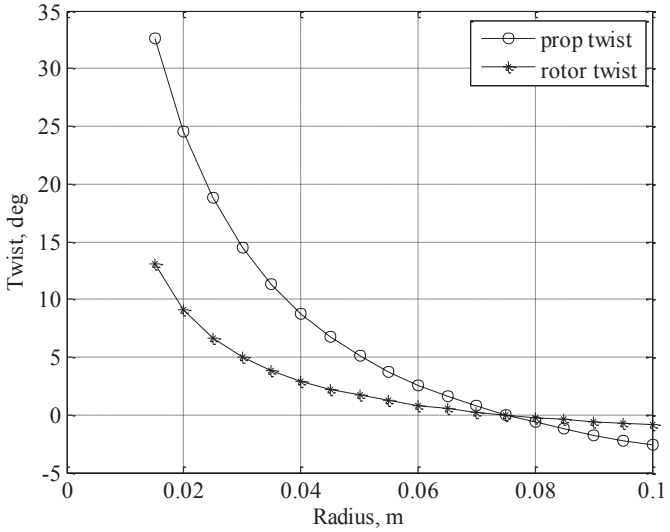

Figure 2: Optimum twist distributions

3. EXLORATION OF PASSIVE TWIST CONTROL

3.1 Concept of centrifugal force induced twist

A deformable, durable and stable blade for MAV proprotor is characterized by the deformation, failure performance and dynamics behavior. To be specific, with respect to the adaptive proprotor of convertible MAV, there are five requirements. Firstly, it should be capable of deforming in terms of twist to adapt different flight conditions. Meanwhile, the deformation should be stable during the rotation. Besides, the design should be practical to be applied on MAV without size problem. Moreover, it can take the airloads without large blade bending. Finally, this adaptive proprotor should have an acceptable fatigue performance.

The initial step of the procedure is to select suitable reinforcing fiber for the laminate blade. The significant factor to select a reinforcing fiber for small-scale proprotor is linked to its tailoring capacity. Glass/epoxy was determined for the MAV flexible proprotor in current study. In order to improve the

aerodynamic performance of flat plate at low Reynolds number, the thickness of laminate blade should be thin enough to provide a low thickness-to-chord ratio [5]. Thus, two typical laminate configurations are considered here, a symmetric laminate $[\theta, -\theta]_T$, and an antisymmetric laminate $[\theta, \theta]_T$. A critical issue in the design of a laminate blade is failure analysis. The comparison of strength of UD and angle-ply laminates was described based on a typical carbon/epoxy composite (AS4/3501-6) using first ply failure analysis [6]. All of the uniaxial tensile strength, uniaxial compressive strength and in-plane shear strength of the angle-ply laminate are evidently higher than those of the off-axis UD material. Thus, in current study, antisymmetric laminates $[\theta, -\theta]_T$ are employed as balanced laminates. The layup of specimen was selected as $[45^\circ, -45^\circ]_T$.

The adaptive proprotor should not only be flexible to produce the required deformation, but also stable to maintain the required twist in each of flight mode. For a stable blade, the blade Center of Gravity (CG) must be ahead of the aerodynamic center [7]. Hence, a concept of centrifugal force induced twist was proposed for adaptive proprotor of convertible MAV. In this concept, tip mass is designed to adjust the global CG of laminate blade. In addition, tip mass is beneficial for improving the nose-down twisting moment and increasing the torsion of laminate blades. On one hand, tip mass is required to be heavy enough to be able to adjust the global CG. On the other hand, it should be light enough to provide weight efficiency for the application on MAVs. Fig. 3 demonstrates the tip mass which can slide in the chordwise direction at blade tip.

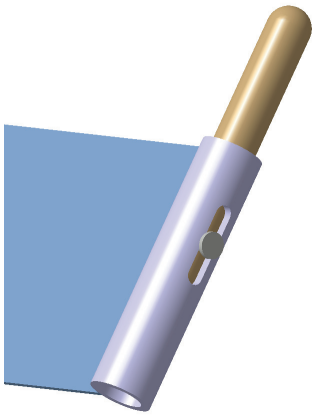

Figure 3: Tip mass model

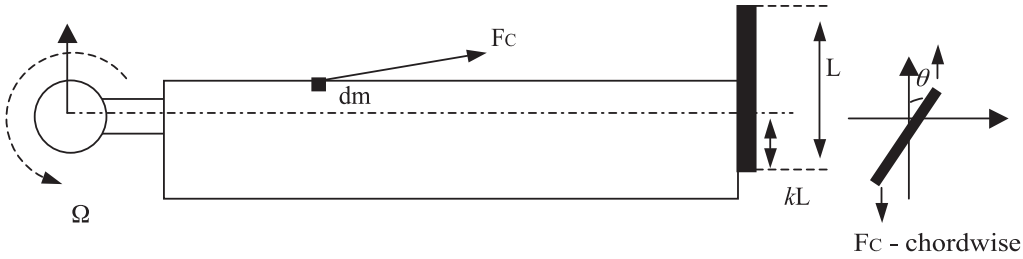

Figure 4: Schematic of Centrifugal Force Induced Twist

The concept of CFIT for adaptive proprotor is described in Fig. 4. The blade is rotating in the anti-clockwise direction in a rotation speed Ω. Factor k is used to define the position of tip rod in the chordwise direction. For example, k=0.5 means that the twisting axis is on the midpoint of tip rod. If k is between 0 and 1, the twisting axis is on the tip rod. Else, the tip rod rotates about the off-body axis. The length of tip rod is represented by L. There is a mass element dm on the rotating blade which can generate a certain centrifugal force F_C. It has a component in the chordwise direction of blade. The component tends to flat the blade cross section with an initial pitch angleθ. This is the method of centrifugal force induced twist blade to generate torsion.

At any local section of blade, the total centrifugal force and total nose-down moment are defined by [13]:

$$F_C(y) = \int_y^R \Omega^2 m_y y dy + m_T \Omega^2 R \tag{3}$$

$$M_{ND}(y) = I_\theta \Omega^2 (R - y) \sin(\theta) + I_T \Omega^2 \sin(\theta_T) \tag{4}$$

Where y is the spanwise coordinates, x represents the chordwise coordinates, R is the proprotor radius, Ω is the rotation speed, m_y is the local mass of laminate blade and m_T is the tip mass. In addition, θ is the local twist angle and θ_T represents the twist angle at the blade tip. The torsional moment of inertia of the blade I_θ is small compared to the torsional moment of inertia of the tip rod I_T, thus the nose-down moment acting on the blade airfoil is negligible compared to the nose-down moment acting on the tip mass. Similarly, the centrifugal force on the blade airfoil is negligible compared to the one on the tip mass. Hence,

$$F_C(y) = m_T \Omega^2 R \tag{5}$$

$$M_{ND}(y) = I_T \Omega^2 \sin(\theta_T) \tag{6}$$

The moment of inertia of the tip rod I_T is defined as:

$$I_T = \int_{-kL}^{(1-k)L} \rho x^2 s dx \tag{7}$$

Changing density ρ with mass m, section area s and rod length L, it becomes:

$$I_T = \frac{m_T}{3L}[((1-k)L)^3 - (-kL)^3] \tag{8}$$

Finally, for a given blade with a tip mass rotating at certain RPM, the nose-down pitching moment can be obtained by Eq. 6. The nose-down pitching moment is expected to help rotating blade to achieve stable deformation and generate the required torsion.

3.2 Global Center of Gravity of laminate blade

In order to achieve the stable deformation of rotating laminate blade, the tip mass was designed to ensure global CG of laminate blade ahead of aerodynamic center. Tab. 3 shows the basic parameters of the blade with tip mass. According to the equilibrium of moment, the global CG of laminate blade can be expressed as a function of position factor *k*. As it can be seen in Fig. 5, with sliding the tip mass forward in the chordwise direction (decreasing factor *k*), the global CG of blade approach the aerodynamic center. After *k*=0.3, the global CG position is ahead of aerodynamic center 0.25, which is

Table 3: The basic parameters on tip mass

Weight of blade (g)	7.0
Weight of tip mass (g)	6.5
Length of tip rod (mm)	35.0
Diameter of tip rod (mm)	5.0
Diameter of tube (mm)	7.0

normalized by the chord of blade. This indicates the tip mass can help to improve the stability of rotating blade.

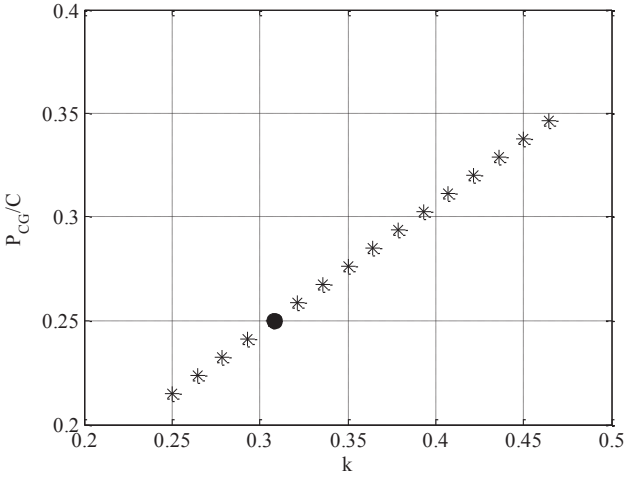

Figure 5: Global CG

3.3 Torsion of rotating laminate blade

The Classical Lamination Theory (CLT) demonstrates that, for a general composite laminate, the forces and moments on it are related to the strains and curvatures at reference surface. The 6 × 6 matrix consisting of the components A_{ij}, B_{ij} and D_{ij} (i, j = 1, 2, 6)is the laminate stiffness matrix, is also called ABD matrix. In order to be able to obtain the strains and curvatures at the reference surface in terms of the force and moment resultants, the ABD matrix is inversed and then becomes the laminate compliance matrix consisting of the components $_{ij}$, and d_{ij} (i, j = 1, 2, 6). The torsion can be directly given by the curvature:

$$k_{xy}^{0} = b_{16}N_x + b_{26}N_y + b_{66}N_{xy} + d_{16}M_x + d_{26}M_y + d_{66}M_{xy} \tag{9}$$

Where N_x, N_y and N_{xy} are the tensile forces in the directions of x, y and xy. Besides, M_x, M_y and M_{xy} represent the moments in varied directions. Terms b_{16}, b_{26}, b_{66}, d_{16}, d_{26} and d_{66} are the corresponding compliance factors.

Since the nose-down pitching moment is obtained, the torsion of rotating laminate blade can be calculated directly using Eq. 9. Fig. 6 gives the blade tip twist of rotating laminate blade with the

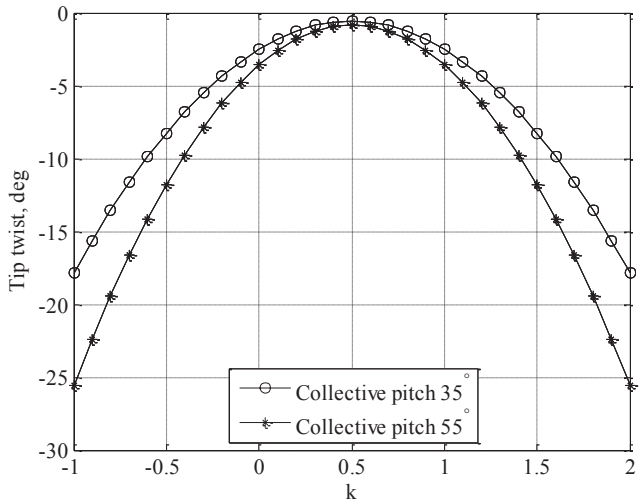

Figure 6: Torsion prediction

variation of tip mass position at 1,500RPM. The torsion of adaptive proprotor is generated at the reasonable level which is between 0 and –30˚.

3.4 Measurement of blade deformation

A key issue to study flexible blade is to use validated predictive simulations and therefore, in the domain of aeroelasticity, to measure accurately deformations. Optical measurement techniques have been developing for some years in aerodynamics, materials and structure, such as Holographic Interferometry (HI), Electronic Speckle Pattern Interferometry (ESPI), Projection Moiré Interferometry (PMI) and Digital Image Correlation (DIC) [8]. In 1998, Fleming obtained the 3-D deformation of rotor blade using PMI technique [9]. However, it has low sensitivity for in-plane deformation and moderate for out-of-plane deformation. By contrast, DIC has a relatively high sensitivity that can reach 1/30,000 of the test field [10]. In 2011, Lawson demonstrated the deformation of a rotating blade using DIC [11]. The technique was found to have many advantages including high resolution results, non-intrusive measurement, and good accuracy over a range of scales. However, DIC needs a preprocessing which is to apply a stochastic speckle pattern to the surface by spraying it with a high-contrast and non-reflective paint. This complex painting will probably affect the stiffness of small MAV blades. Hence, in this study, LDS based method was developed to measure blade deformation in both of hover and forward flight.

The final laminate blades with tip masses are shown in Fig. 7. The bending and torsion distributions during rotation are considered as the blade deformation, since beneficial torsion can increase the overall performance while bending tends to decrease the thrust. In order to measure the deformation of rotating laminate blade, a laser displacement sensor system was developed, as shown in Fig. 8. To avoid any disturbance on flow field, the two laser displacement sensors were fixed at an incidence angle to measure the blade deformation. The laser displacement sensor used in this experiment is a KEYENCE LK-G502. The sampling frequency was set to 10,000Hz. Diffuse reflection mode of laser displacement sensor was used for measurements. The distance of reference was 500mm, and the range of measuring was between -250mm to 500mm. For a long range measurement, the measuring accuracy is typically ±0.1% of Full Scale (FS). In order to reconstruct the deformed blade and to extract the bending and torsion, the post-processing methodology based on polynomial surface fitting was developed for LDS technology. The adaptive proprotor were respectively tested in rotor mode, 1,100RPM, 1,300RPM and propeller mode, inflow velocity 8m/s, 800RPM (limited by current motor). The position factor k of tip mass on adaptive proprotor was set to 0.25. The results were compared with the predictions from a Fluid Structure Model (FSI) which was based on the combination of BEMT and beam model.

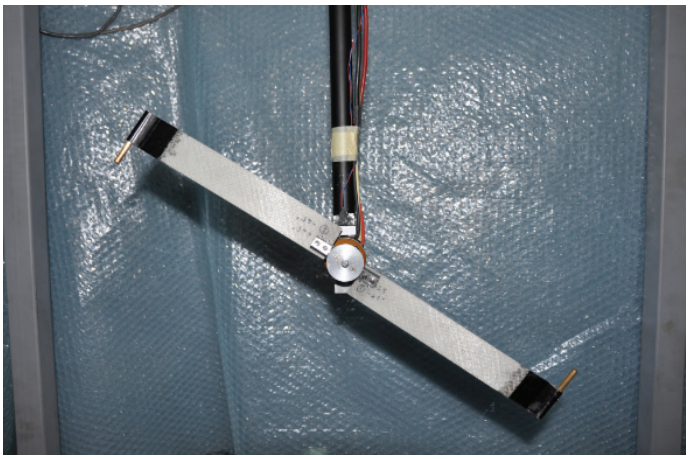

Figure 7: Adaptive proprotor

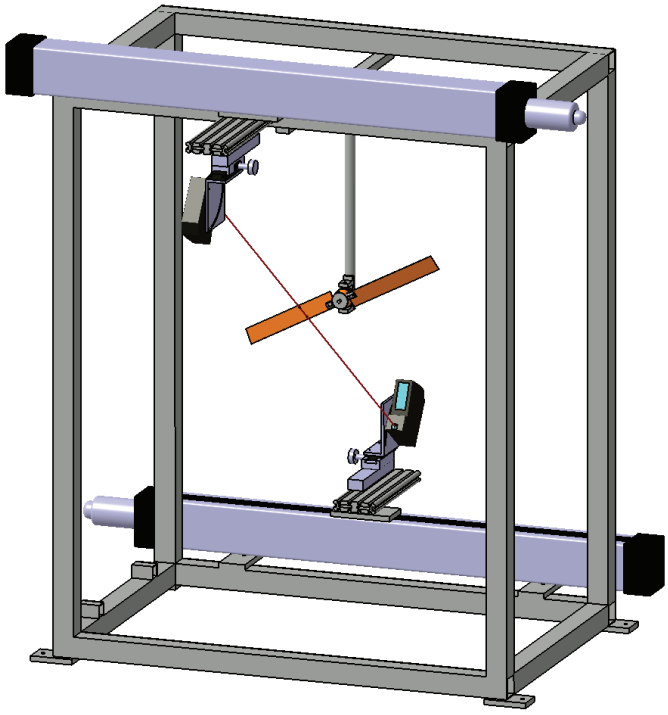

Figure 8: LDS rig

The detailed bending and torsion were extracted according to surface function and shown in Figs. 9 and 10. The experimental results were plotted with 95% confidence bounds of the fitting. In rotor mode, with increasing RPM, the bending from measurements decreased obviously due to the centrifugal stiffening effect (Figs. 9(a), 9(b)). By contrast, the torsion from measurements increases by high nose-down pitching moment of increased RPM (Figs. 10(a), 10(b)). FSI model also reveals this phenomenon in rotor mode. As it can be seen from the results of experiments and FSI model (Fig. 9(c)), even RPM is only 800 (low RPM has no strong stiffening effect), the bending still is relatively low due to the

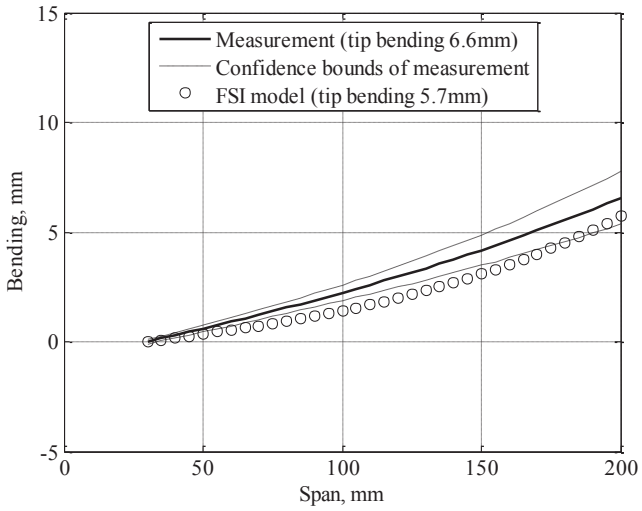

(a) Rotor mode: 1,100RPM

Figure 9: *(Continued)*

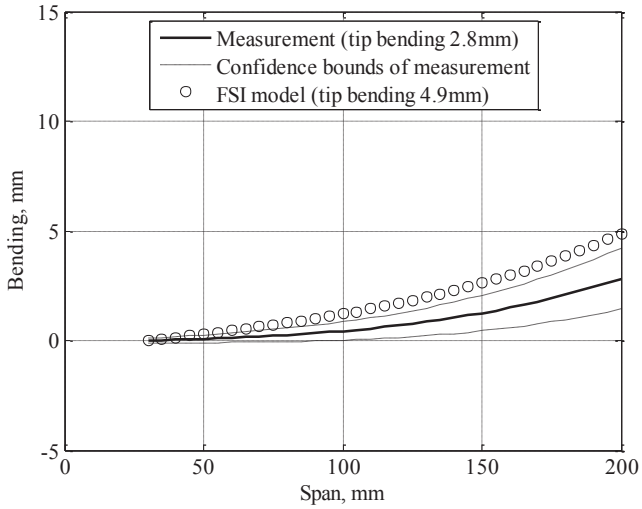

(b) Rotor mode: 1,300RPM

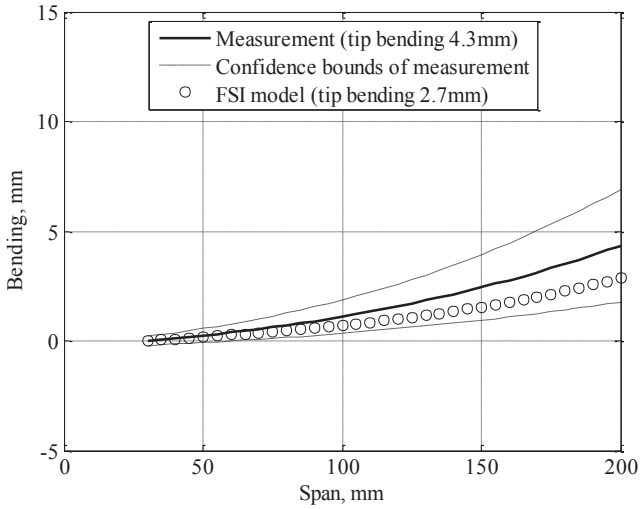

(c) Propeller mode: 800RPM, inflow 8m/s

Figure 9: Bending distribution

inflow airloads acting on the blade. The torsion is also low since there was no adequate nose-down pitching moment in this case (Fig. 10(c)). It was found that the centrifugal force induced twist blade is capable of generating negative torsions in two modes. Besides, in propeller mode, the laminate blade can take airloads without large negative bending.

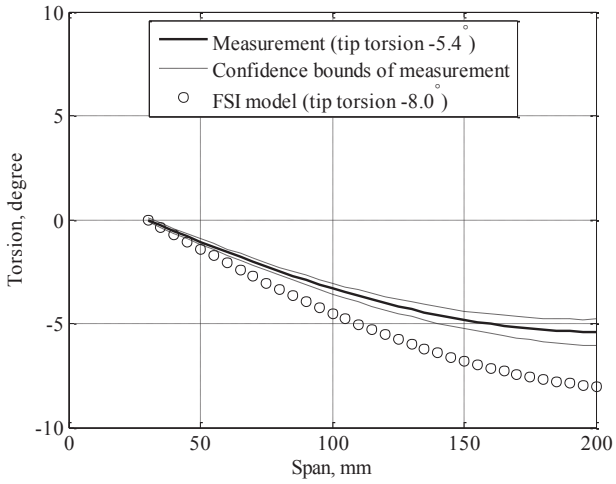

(a) Rotor mode: 1,100RPM

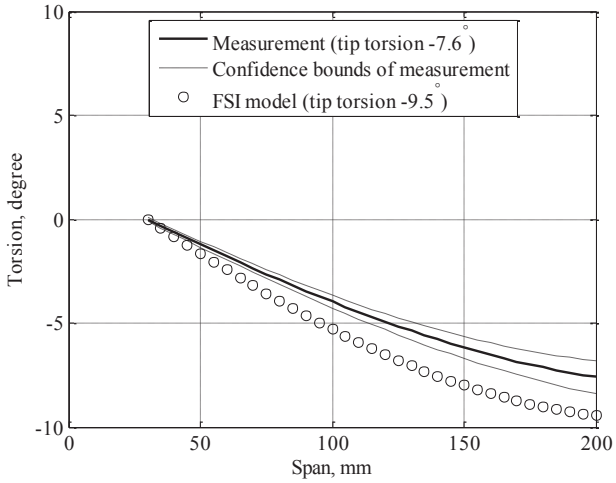

(b) Rotor mode: 1,300RPM

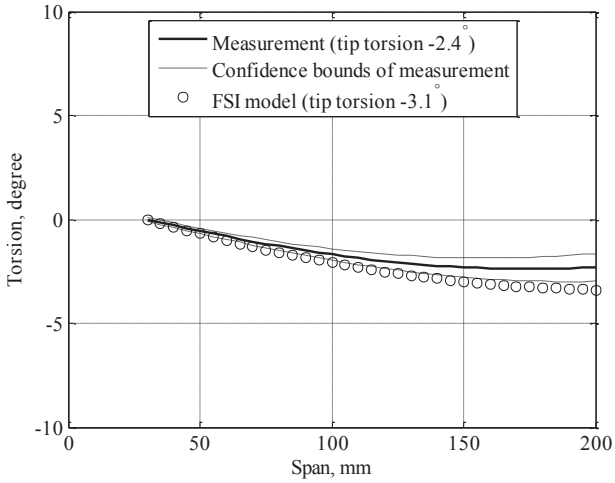

(c) Propeller mode: 800RPM, inflow 8m/s

Figure 10: Torsion distribution

4. APPLICATIONS ON MAVION

Since the adaptive proprotor showed the potential negative torsion generated respectively in rotor and propeller mode, hence, this concept was applied on MAVion. Based on the geometry of widely used APC86 commercial propeller with a diameter 0.2m (Fig. 11), a rigid blade, a rigid blade with collective pitch control and an adaptive blade with collective pitch control were compared using BEMT [12, 13]. The detailed chord and twist distributions of APC86 are given by Figs. 12 and 13.The twist distribution of APC86 exhibits the bi-linear behavior. The root twist of rigid APC86 is around 45˚ and the tip twist is 20˚. In order to compare the adaptive concept with current propeller on MAVion, two additional linear twist distributions are defined, based on –10˚ and –30˚ of global twist.

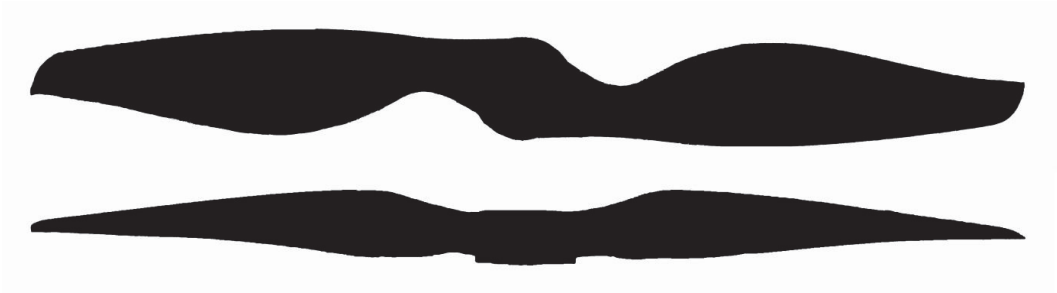

Figure 11: Top and side views of APC86

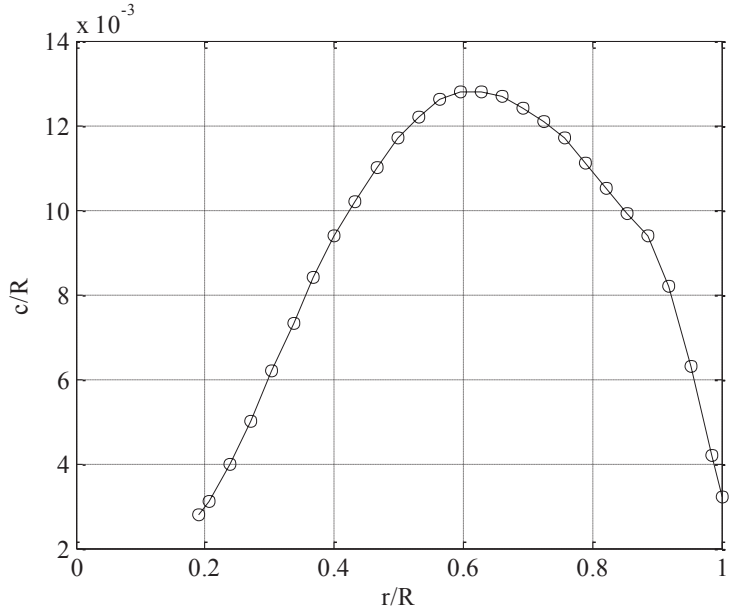

Figure 12: Chord distribution of APC86

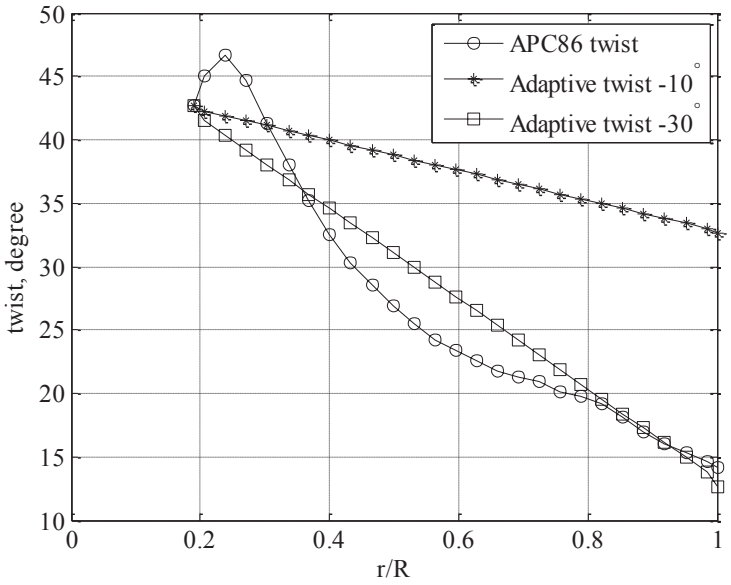

Figure 13: Twist distributions of APC86 and potential adaptive blades

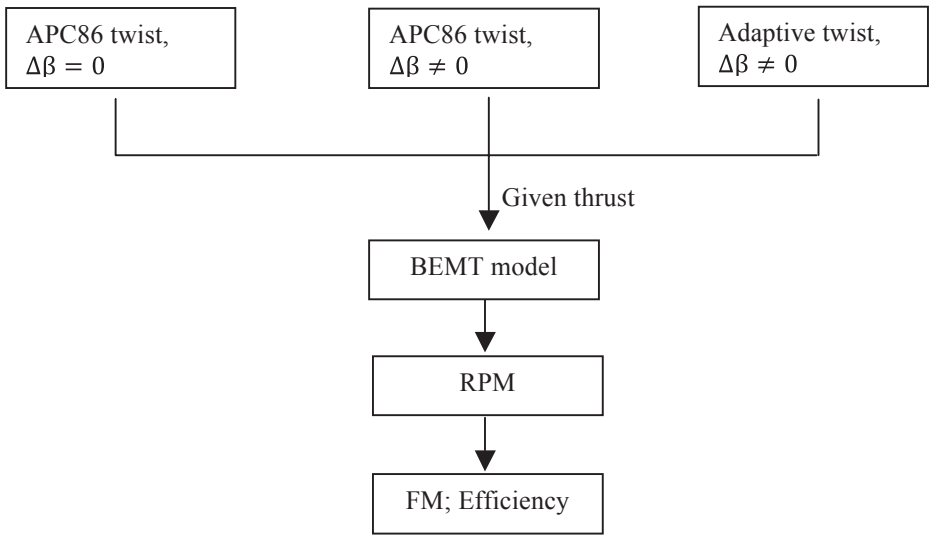

Figure 14: Program of evaluating potential benefits of adaptive twist

$\Delta\beta$ represents the variation of collective pitch. APC86 rigid blade without collective pitch control ($\Delta\beta = 0$) was inputted to BEMT model to find a RPM which can provide 2N for hover and 0.3N for forward flight.APC86 rigid blade with collective pitch control ($\Delta\beta \neq 0$) means the APC86 rigid blade was mounted with different collective pitches. A number of RPMs were obtained by BEMT model to achieve the given thrusts for each collective pitch. On the adaptive blade with collective pitch control ($\Delta\beta \neq 0$), the blades with two potential twist distributions –10° and –30° were analyzed with a series of collective pitches through BEMT model respectively. With the required thrusts, the corresponding RPMs were obtained. Finally, FM and propulsive efficiency can be calculated and compared in both rotor and propeller modes (Fig. 14).

The marker ● corresponds to the APC86 rigid blade without collective pitch control. The curve with marker ○ shows the required RPMs of APC86 rigid blade for different collective pitches in each mode. Fig. 15 demonstrates the required RPM for the cases discussed above to achieve 2N for rotor mode. As can be seen, 6,500RPM is required to reach the thrust target ($\Delta\beta = 0$).In Fig. 16, the APC86 rigid blade without collective pitch control needs around 6,000RPM to obtain the thrust 0.3N at inflow velocity

16m/s in propeller mode ($\Delta\beta = 0$).In both modes, with reducing collective pitch, RPM is needed to increase for the given thrust. The two blades with adaptive twist distributions –10˚ and –30˚ also suggest the same trend.

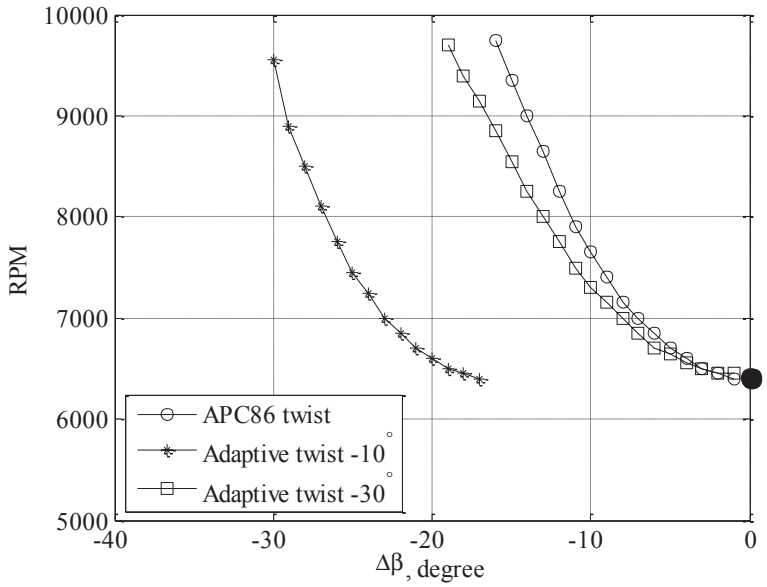

Figure 15: The required RPMs for given thrust 2N in rotor mode

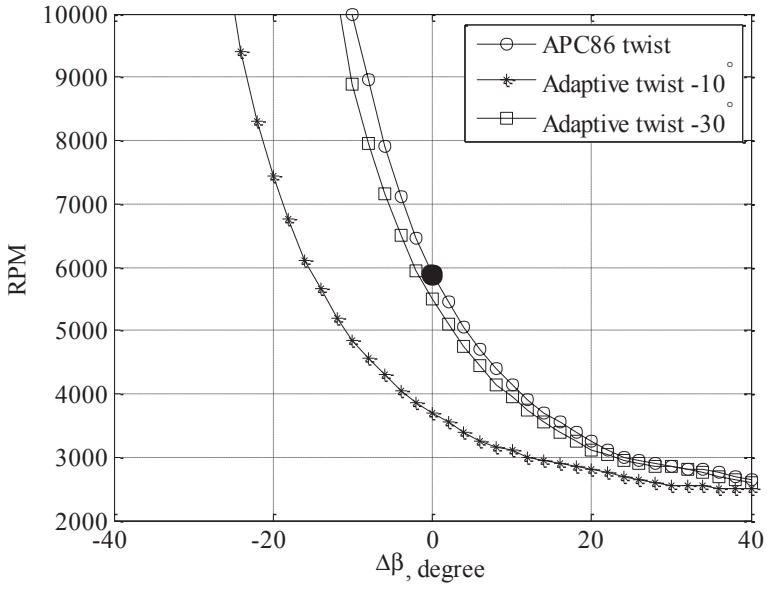

Figure 16: The required RPMs for given thrust 0.3N in propeller mode (inflow 16m/s)

Fig. 17 gives the FM comparison among three cases in rotor mode. For APC86 rigid blade, the FM is approximately 0.57 when 2N thrust is provided. With additional collective pitch control, the maximum value of FM is 0.65 where is variation of collective pitch $\Delta\beta = -7^{\circ}$. The FM peak of blade with adaptive twist –30˚ is lower than APC86 rigid blade with collective pitch control. However, the blade with adaptive twist –10˚ has the maximum value of FM 0.68. This indicates, using adaptive blade with collective pitch control which can generate –10˚ torsion can improve the FM more than using rigid blade with collective pitch control. The propulsive efficiencies are compared in Fig. 18 for propeller

mode. For the APC86 rigid blade without collective pitch control, the propulsive efficiency is 0.6. When the APC86 rigid blade is with collective pitch control, the peak of propulsive efficiency becomes 0.7 at $\Delta\beta = 15^\circ$.

The adaptive blade with collective pitch control which can generate torsion –30° has the same efficiency peak with APC86 rigid blade with collective pitch control, since the original twist of APC8X6 is relatively high with a bi-linear –45°.

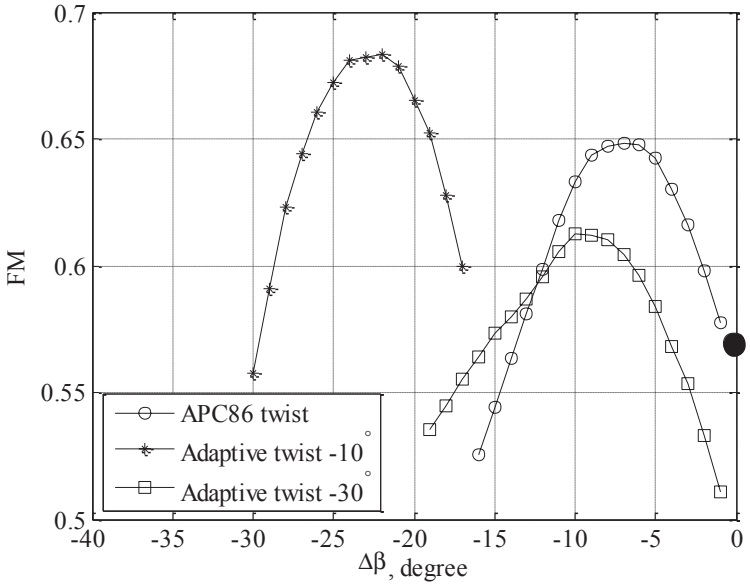

Figure 17: FM comparison in rotor mode

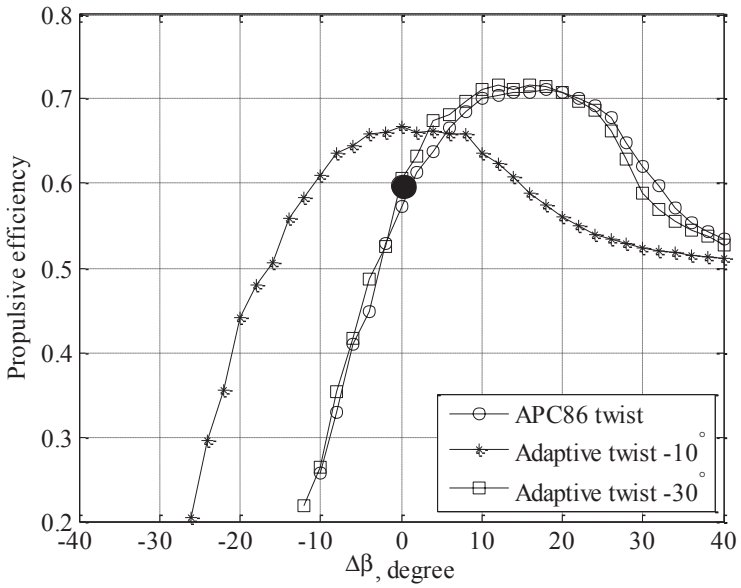

Figure 18: Propulsive efficiency comparison in propeller mode

CONCLUSION

To adapt different flight modes and increase the overall efficiency for convertible MAV, a centrifugal force induced twist concept of adaptive blade was proposed in present study. A glass fiber laminate blade with stacking sequence $[45^\circ, 45^\circ]_T$ was used for adaptive proprotor. Meanwhile, tip mass was designed to increase the stability by ensuring the global CG ahead of aerodynamic center, and to

generate negative torsion by increasing nose-down pitching moment. LDS rig and corresponding post-processing method were implemented to measure the deformation of rotating blade. The feasibility of adaptive blade was verified since the negative torsion was observed respectively in rotor and propeller mode. The potential adaptive proprotor which can generate –10˚ torsion has the peak of FM in rotor mode. In propeller mode, the blade with –30˚ has the same maximum value of efficiency with APC86 rigid propeller of bi-linear twist. The application of adaptive blade is not only in aerodynamic efficiency but also in dynamic performance. In the next study, an optical derotator, a sophisticated tool for performing non-contact vibration measurements on rotating parts with laser vibrometers, will be employed to study the dynamic response of rotating adaptive proprotor for MAVion. In addition, the aerodynamic performance is also going to be tested in each mode.

ACKNOWLEDGEMENTS

This work is supported by the China Scholarship Council(CSC) and Malaysian Ministry of Higher Education (MOHE). The authors thank Rémy CHANTON and Xavier FOULQUIER for their support in conducting the experiments.

REFERENCES

[1] S. Shkarayev, J. M. Moschetta and B. Bataille, Aerodynamic Design of Micro Air Vehicles for Vertical Flight, *Journal of Aircraft*, Vol. 45, No. 5, 2008, pp. 1715-1724.

[2] M. A. McVeigh, H. J. Rosenstein and F. J. McHugh, Aerodynamic Design of the XV-15 Advanced Composite Tilt Rotor Blade, *39th Annual Forum of the American Helicopter Society*, St. Louis, MO, May 1983.

[3] M. W. Nixon, Improvements to Tilt Rotor Performance through Passive Blade Twist Control, *NASA Technical Memorandum 100583*, April 1988.

[4] B. J. Hein and I. Chopra, Hover Performance of a Micro Air Vehicle: Rotors at Low Reynolds Number, International Specialists Meeting Unmanned Rotorcraft: Design, Control ans Testing, *Chandler, AZ*, January 2005.

[5] M. Drela, XFOIL 6.9 User Guide, *Massachusetts Institute of Technology*, 2001.

[6] I. M. Daniel and O. Ishai, Engineering Mechanics of Composite Materials, Oxford University Press 1994.

[7] J. Sicard, Investigation of an Extremely Flexible Stowable Rotor for Micro-helicopters, Master's thesis, *University of Texas at Austin*, May 2011.

[8] S. Rajpal, Optical Methods of Measurement: Whole-field Techniques, Second edition, *Francis and Taylor*/CRC Press, 2009.

[9] G. A. Fleming and S. Gorton, Measurement of Rotorcraft Blade Deformation Using Projection Moiré Interferometry, Proceedings of the 3rd International Conference on Vibration Measurements by Laser Techniques: Advances and Applications, SPIE the International Society for Optical Engineering, *Ancona*, Italy, June 1998, pp. 514-527.

[10] T. Schmidt and J. Tyson, Full-Field Dynamic Displacement and Strain Measurement Using Advanced 3D Image Correlation Photogrammetry: Part 1, *Experimental Techniques*, Vol. 27, No. 3, 2003, pp. 47-50.

[11] M. S. Lawson and J. Sirohi, Measurement of Deformation of Rotating Blades Using Digital Image Correlation, Proceedings of 52nd AIAA/ASME/ASCE/AHS/ASC Structures, *Structural Dynamics and Materials Conference*, Denver, Colorado, April 2011.

[12] J. G. Leishman, Principles of Helicopter Aerodynamics, *Cambridge Aerospace Series*, 2nd edition, 2006.

[13] P. Lv, S. Prothin, F. M. Zawawi, E. Benard, Joseph Morlier and J. M. Moschetta, Study of A Flexible Blade for Optimized Proprotor, ERCOFTAC International Symposium, *Unsteady Separation in Fluid-Structure Interaction*, Mykonos, Greece, June 2013.

[14] F. Moha-Zawawi, S. Prothin, P. Lv, E. Benard, J. M. Moschetta and J. Morlier, Study of a flexible UAV proprotor *48th International Symposium of Applied Aerodynamics Saint-Louis*, Vol. 30, 2013, pp. 1-10.